Scientific Research Publishing

Journal of Materials Science and Chemical Engineering, 2024, 12, 40-52
https://www.scirp.org/journal/msce
ISSN Online: 2327-6053
ISSN Print: 2327-6045

Investigation of the Micro-Mechanics of an Extruded Precipitation-Strengthened Magnesium Alloy under Cyclic Loading

Chuhao Liu[1], Xiaodan Zhang[1], Huamiao Wang[2*], Yinghong Peng[1]

[1]State Key Laboratory of Mechanical System and Vibration, Shanghai Jiao Tong University, Shanghai, China
[2]School of Mechanics and Engineering Science, Shanghai University, Shanghai, China
Email: *wanghm@shu.edu.cn

How to cite this paper: Liu, C.H., Zhang, X.D., Wang, H.M. and Peng, Y.H. (2024) Investigation of the Micro-Mechanics of an Extruded Precipitation-Strengthened Magnesium Alloy under Cyclic Loading. *Journal of Materials Science and Chemical Engineering*, **12**, 40-52.
https://doi.org/10.4236/msce.2024.127004

Received: June 26, 2024
Accepted: July 28, 2024
Published: July 31, 2024

Abstract

Precipitation strengthening is a crucial microscopic mechanism for enhancing the strength of magnesium alloys. In order to elucidate the influence of precipitation on the microscopic deformation mechanisms and macroscopic mechanical response of magnesium alloys under cyclic loading conditions, we employed a crystal plasticity model to analyze the stress-strain curves, specific crystal plane diffraction intensities, and the temporal evolution of various microscopic deformation mechanisms and twinning volume fractions for an extruded magnesium alloy, AXM10304, containing coherent precipitates. The research findings indicate that precipitation does not fundamentally alter the microscopic mechanisms of this alloy. However, it hinders twinning during the compression stage, mildly promotes detwinning during the tension stage, and enhances tension secondary hardening by elevating the difficulty of activation of the prismatic slip.

Keywords

Cyclic Deformation, Magnesium Alloy, *In-Situ* Neutron Diffraction, Precipitation Strengthening, Crystal Plasticity, Lattice Strain, Mechanism Evolution

1. Introduction

Magnesium alloys, characterized by low density, high specific strength, and good damping properties, represent potential structural materials in the field of engineering [1]. However, its widespread application is limited by its relatively low absolute strength. By introducing precipitates, it is possible to strengthen mag-

nesium alloys. For example, Peng *et al.* [2] developed a special aging process that includes an externally applied stress field, introducing spherical precipitate particles into Mg-5wt.%Sc alloy. This process resulted in an improvement in both the strength and toughness of the alloy. Agnew *et al.* [3] also investigated the macro- and micro-mechanical behavior of Mg-Y-Nd-Zr alloy WE34 in the solution-treated, peak-aged, and over-aged states through a combination of *in-situ* neutron diffraction and simulations. They found that precipitation strengthening is more pronounced for basal slip, resulting in a relatively limited enhancement of the overall strength of the alloy. Additionally, Rosalie *et al.* [4] employed a process combining pre-aging deformation and peak aging to investigate the influence of rod-shaped precipitates on the strength and toughness of Mg-Zn alloys with extruded textures. Their study indicated that rod-shaped precipitates could provide an approximately 13.2% increase in strength, but plasticity would be reduced by more than half. Research on precipitation-strengthened magnesium alloys has largely focused on simple uniaxial tension or compression processes. However, there is a relative scarcity of studies on the effects of precipitates on macroscopic and microscopic mechanical behavior under cyclic loading. This is due to the complex microstructural plastic deformation mechanisms of magnesium alloys, making the investigation of their fatigue behavior relatively challenging. Magnesium alloys possess a hexagonal close-packed (HCP) crystal structure with poor symmetry. Plastic deformation in these alloys is typically coordinated through mechanisms such as basal slip, prismatic slip, pyramidal slip, and tensile twinning. Consequently, pronounced tension-compression asymmetry often occurs during cyclic loading, especially when a strong texture is present [5]-[9]. However, there is still insufficient research on the relationship between the microscale mechanisms and macroscopic stress-strain response of magnesium alloys during cyclic loading in the presence of precipitates.

Recently, Xie *et al.* [10] [11] conducted *in-situ* characterization experiments to preliminarily analyze the impact of precipitation strengthening on the cyclic mechanical behavior of magnesium alloys. They initially revealed the alternating mechanisms of twinning and detwinning in the microstructure. However, experimental methods alone are insufficient to distinguish the impact of individual dislocation slip mechanisms and the twinning shear mechanism on macroscopic mechanical responses. Additionally, they cannot quantitatively describe the influence of precipitates on these mechanisms. Crystal plasticity models are essential tools for investigating the connection between microscale mechanisms and macroscopic mechanical properties of alloys and have been successfully applied to the analysis of magnesium alloys. Through such models, well-established mapping relationships have been established between various microscale plastic deformation modes and the mechanical responses to uniaxial deformation in magnesium alloys [3] [12] [13]. Nevertheless, the current models utilized in reported works have not yet taken into account the effects of precipitation strengthening, and there is a lack of simulations specifically tailored for multi-cycle loading conditions. To further elucidate the influence of precipitation

strengthening on various plastic deformation mechanisms and the mechanical response of precipitation-strengthened magnesium alloys under cyclic loading, this work employed a crystal plasticity model capable of distinguishing processes such as twinning nucleation, growth, and contraction. The temporal evolution of different deformation mechanisms during the cyclic loading process, the impact of precipitates, and the resultant macroscopic stress-strain curves were investigated.

2. Materials and Modeling Methods

The extruded precipitation-strengthened magnesium alloy under investigation in our study is designated as AXM10304. We utilized relevant experimental data previously published by Xie *et al.* [11]. The specific composition of this alloy is Mg-1.3Al-0.3Ca-0.4Mn (weight percent, wt.%). They categorized the alloy into two groups of specimens based on whether they underwent peak aging heat treatment. Specimens subjected solely to a 500˚C solution treatment for 10 minutes are referred to as the solution-state sample (denoted as ST sample), whereas the control group, subsequently subjected to aging treatment at 200˚C, is designated as the peak-aged sample (denoted as PA sample), which possesses a coherent precipitate strengthening phase. Our model was similarly simulated for each of the two specimen types separately. Furthermore, we predominantly chose experimental data from the initial compression, 1st cycle, 2nd cycle, 5th cycle, and 10th cycle, comparing them with the simulation results. Xie *et al.* [11] also conducted *in-situ* neutron diffraction experiments, as illustrated in **Figure 1(a)**. Neutron diffraction allows the acquisition of diffraction intensity evolution data for specific crystal planes during cyclic tension-compression experiments, which is subsequently applied for the validation of our model predictions. Other detailed information about the materials processing and microstructures are described in detail in Nakata *et al.* [14].

To investigate the relationship between the microscale mechanical behavior and the macroscale mechanical response of precipitation-strengthened magnesium alloys, our primary research approach involves the use of crystal plasticity models. Our work adopts the elasto-viscoplastic self-consistent model (denoted as EVPSC-TDT) proposed by Wang *et al.* [15] [16]. Due to space constraints, we provide only a concise overview of the model in this section. This model treats the entire material as a homogeneous polycrystalline aggregate, in which each grain is embedded as an equivalent ellipsoid inclusion, as shown in **Figure 1(b)**. By solving the constitutive model of each grain and the homogeneous polycrystalline aggregate, as well as the interaction between them, this model can predict the micro- and macro-mechanical responses of the material. For a specific micro deformation system, α (e.g., dislocation slip or twinning) in an individual grain, the shear rate, $\dot{\gamma}^{\alpha}$, could be express as

$$\dot{\gamma}^{\alpha} = \dot{\gamma}_0 \left| \frac{\tau^{\alpha}}{\tau_c^{\alpha}} \right|^{1/m} \operatorname{sgn}\left(\tau^{\alpha}\right) \tag{1}$$

where $\dot{\gamma}^0$, τ^α, τ_c^α, and m represents the reference value of shear rate, resolved shear stress (RSS), critical resolved shear stress (CRSS), and strain rate sensitivity (SRS) exponent, respectively. Interestingly, for mechanisms related to twinning, such as twinning nucleation, growth, and contraction, their corresponding CRSS should differ.

This is natural, as the nucleation difficulty is inherently higher from a physical perspective compared to growth. To address this, our EVPSC-TDT model takes into account the activation difficulties associated with the three distinct stages of the twinning mechanism mentioned above. For twinning nucleation, the shear strain rate and twinning volume fraction (TVF) rate is expressed respectively as

$$\dot{\gamma}_{ini}^{\alpha} = \begin{cases} \dot{\gamma}_0 \left| \dfrac{\tau^\alpha}{\tau_c^{ini}} \right|^{1/m}, \left(\tau^\alpha > 0\right) \\ 0, \left(\tau^\alpha \le 0\right) \end{cases} \tag{2}$$

$$\dot{f}_{ini}^{\alpha} = \left|\dot{\gamma}_{ini}^{\alpha}\right| / \gamma^{tw} \tag{3}$$

where γ^{tw} (=0.129) is the characteristic twinning shear of Mg alloys. Similarly, for the twinning growth stage, our model separately considers the shear strain rates in the parent and twin crystals as

$$\dot{\gamma}_{gro,parent}^{\alpha} = \begin{cases} \dot{\gamma}_0 \left| \dfrac{\tau^\alpha}{\tau_c^{gro}} \right|^{1/m}, \left(\tau^\alpha > 0\right) \\ 0, \left(\tau^\alpha \le 0\right) \end{cases} \tag{4a}$$

$$\dot{\gamma}_{gro,child}^{\alpha} = \begin{cases} -\dot{\gamma}_0 \left| \dfrac{\tau^\alpha}{\tau_c^{gro}} \right|^{1/m}, \left(\tau^\alpha < 0\right) \\ 0, \left(\tau^\alpha \ge 0\right) \end{cases} \tag{4b}$$

The calculation of the TVF rate is given by

$$\dot{f}_{gro}^{\alpha} = f^P \left|\dot{\gamma}_{gro,parent}^{\alpha}\right| / \gamma^{tw} + f^\alpha \left|\dot{\gamma}_{gro,child}^{\alpha}\right| / \gamma^{tw} \tag{5}$$

where f^α is the volume fraction of the α-th twinning variant, and f^P ($=1-\sum f^\alpha$) is the volume fraction of the parent grain. In a similar fashion, for twinning contraction, we can also calculate the corresponding shear strain rate and TVF rate as

$$\dot{\gamma}_{dtw,parent}^{\alpha} = \begin{cases} -\dot{\gamma}_0 \left| \dfrac{\tau^\alpha}{\tau_c^{dtw}} \right|^{1/m}, \left(\tau^\alpha < 0\right) \\ 0, \left(\tau^\alpha \ge 0\right) \end{cases} \tag{6a}$$

$$\dot{\gamma}_{dtw,child}^{\alpha} = \begin{cases} \dot{\gamma}_0 \left| \dfrac{\tau^\alpha}{\tau_c^{dtw}} \right|^{1/m}, \left(\tau^\alpha > 0\right) \\ 0, \left(\tau^\alpha \le 0\right) \end{cases} \tag{6b}$$

$$\dot{f}_{dtw}^{\alpha} = -f^P \left|\dot{\gamma}_{dtw,parent}^{\alpha}\right| / \gamma^{tw} - f^\alpha \left|\dot{\gamma}_{dtw,child}^{\alpha}\right| / \gamma^{tw} \tag{7}$$

During deformation, the evolution of CRSS for both dislocation glide and twinning related mechanisms, $\dot{\tau}_c^\alpha$, could be calculated by the following equation as

$$\dot{\tau}_c^\alpha = \mathrm{d}\frac{\hat{\tau}^\alpha}{\mathrm{d}\Gamma}\sum_\beta h^{\alpha\beta}\dot{\gamma}^\beta \tag{8}$$

where Γ refers to the accumulated shear strain. $\dot{\gamma}^\beta$ is the shear rate of the neighbor deformation system, β, and $h^{\alpha\beta}$ is the latent hardening parameter which represents the obstacle effect of adjacent deformation system on α. In addition, $\hat{\tau}^\alpha$ is a threshold value of CRSS in α, which obeys an extended Voce hardening law as

$$\hat{\tau}^\alpha = \tau_0^\alpha + \left(\tau_1^\alpha + h_1^\alpha\Gamma\right)\left\{1-\exp\left(-\frac{h_0^\alpha}{\tau_1^\alpha}\Gamma\right)\right\} \tag{9}$$

where τ_0^α, h_0^α, h_1^α, and $\tau_0^\alpha+\tau_1^\alpha$ is the initial CRSS, initial hardening rate, asymptotic-hardening rate, and back-extrapolated CRSS, respectively. These parameters can be determined by experimental results. One can get more detailed description of the EVPSC framework from the previous work [15]-[18].

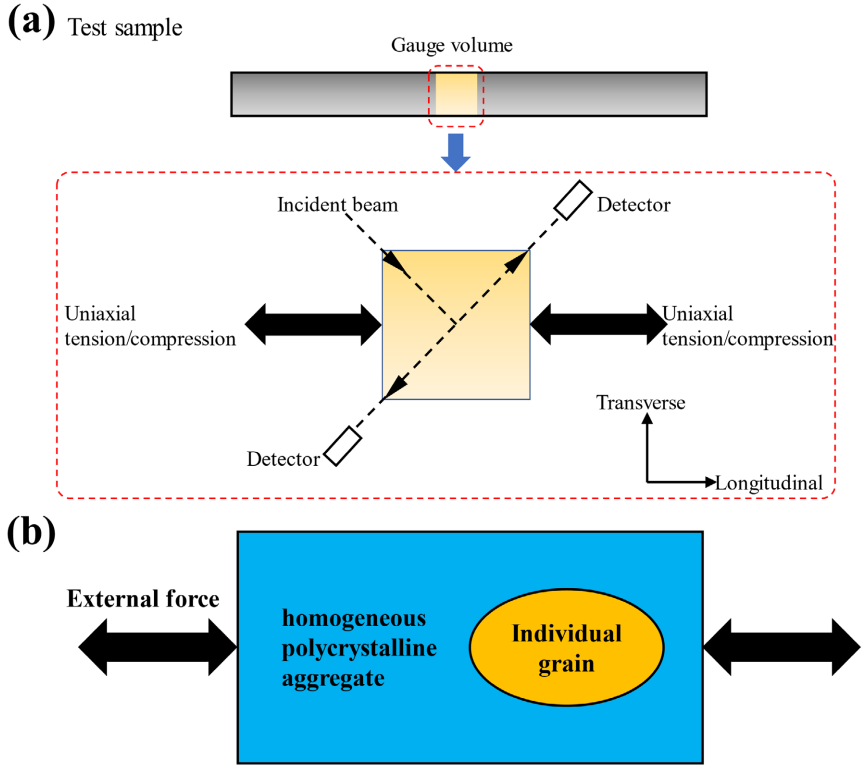

Figure 1. Schematic diagrams illustrating the principles of (a) the cyclic loading test accompanied by the *in-situ* neutron diffraction and (b) the EVPSC-TDT modeling framework.

3. Results

Leveraging published experimental data and the EVPSC-TDT model consider-

ing the differences in twinning nucleation, growth, and contraction, we investigated the interplay between the microscale deformation mechanisms and the macroscopic mechanical response under cyclic loading for the precipitation-strengthened magnesium alloy AXM10304. The stress-strain curves for both the ST and PA samples during the initial compression, 1st cycle, 2nd cycle, 5th cycle, and 10th cycle are depicted in **Figure 2**, showing experimental and predicted results. As evident from the figure, the simulation results closely align with the experimental data, validating the reliability of the model parameters, which are listed in **Table 1**. The letters, A to F, in **Figure 2** refer to different states during cyclic loading. Both the ST and PA samples exhibit certain commonalities in their macroscopic stress-strain curves. For instance, both specimens exhibit pronounced tension-compression asymmetry. The strain hardening rate during the compression stage (A-B and G-B) is significantly smaller than the strain hardening rate during the secondary hardening stage (D-E) in tension. This results in the compressive peak stress being lower than the tensile peak stress. With an increase in the number of cycles, the peak stresses at points B and E also gradually increase. Additionally, both of them exhibit an S-shaped curve during the reverse tension stage. This phenomenon is associated with the alloy's detwinning mechanism (*i.e.*, the twin contraction) [19]. Certainly, there

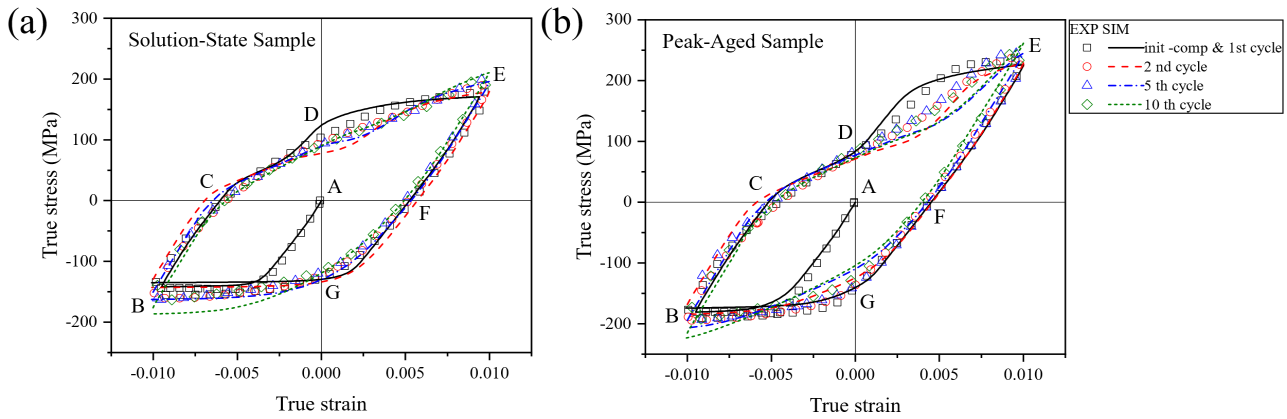

Figure 2. The experimental and predicted true stress-strain curves within the initial compression, 1st cycle, 2nd cycle, 5th cycle, and 10th cycle for the (a) ST sample and (b) PA sample.

Table 1. The hardening parameters specified in the EVPSC-TDT model. Only the initial CRSS, τ_0, was considered for a tensile-twinning mode with respect to the different regimes during cyclic loading. Values of the asymptotic-hardening rate, h_1, are all set to be zero and not listed. All values are in MPa.

Sample	Deformation mode											
	Basal <a>			Prismatic <a>			Pyramidal <c + a>			Extension twin		
	τ_0	τ_1	h_0	τ_0	τ_1	h_0	τ_0	τ_1	h_0	τ_0^{ini}	τ_0^{gro}	τ_0^{dtw}
ST	10	17	59	72	65	87	90	150	350	69	53	19
PA	15	50	61	97	77	180	100	650	923	78	60	22

are also notable differences between the two. The peak stress of the PA specimens is significantly higher than that of the ST specimens, which is associated with the strengthening effect of precipitates. As shown in **Table 1**, the presence of precipitates hinders dislocation slip and twinning shear, resulting in an increase in their respective CRSS. On a macroscopic level, this translates to the need for higher external stress levels to activate these microscale deformation mechanisms.

The tension-compression asymmetry of the alloy is related to its microscale plastic deformation modes. In this regard, information on the diffraction intensity of specific crystal planes provides evidence. *In-situ* neutron diffraction experiment results depict the evolution of diffraction intensity for three crystal planes during cyclic loading in the initial compression, 1st cycle, 2nd cycle, 5th cycle, and 10th cycle, and are compared with simulation results, as shown in **Figure 3**. As evident from the figure, the experimental and simulated results for both types of samples are in good agreement. From **Figure 3(a)**, it can be observed that the evolution patterns of crystal planes {10.0} and {11.0} in the ST specimens follow a similar trend, while they are precisely opposite to the evolution pattern of plane {00.2}. It is noteworthy that the diffraction intensity of the {00.2} crystal plane can be used to trace the twinning and detwinning mechanisms of the alloy [10]. The increase in diffraction intensity of the {00.2} crystal plane signifies an increase in the TVF, while a decrease indicates a reduction in the TVF. These changes correspond to the alternating dominance of the twinning and detwinning mechanisms. This alternating mechanism of twinning and detwinning contributes to the tension-compression asymmetry observed during the cyclic

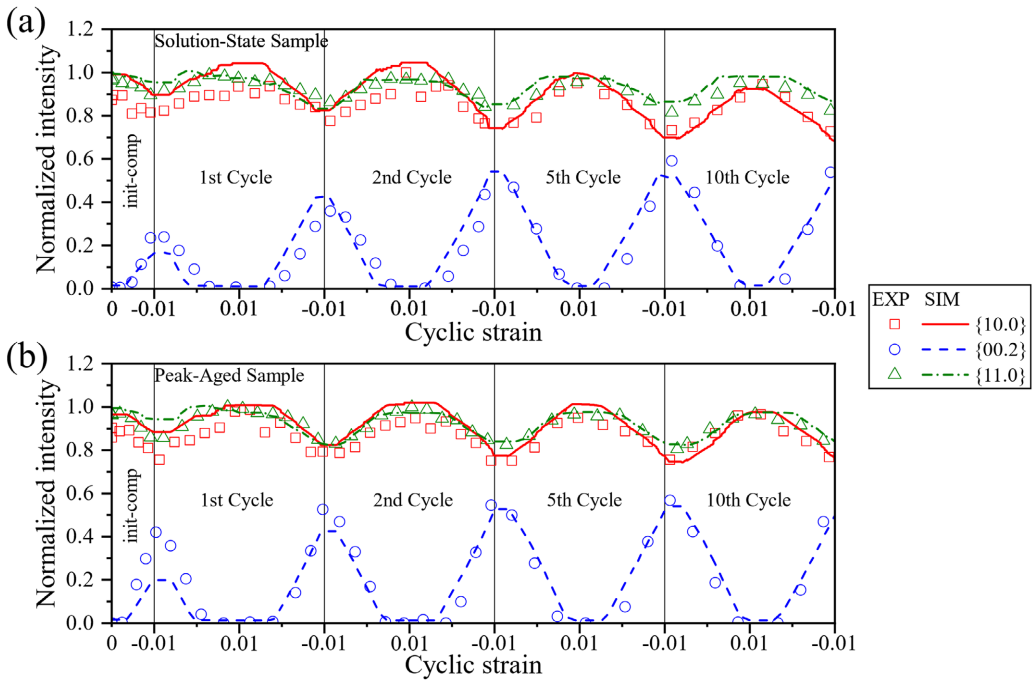

Figure 3. The experimental and predicted normalized intensity versus the cyclic strain within the initial compression, 1st cycle, 2nd cycle, 5th cycle, and 10th cycle for the (a) ST sample and (b) PA sample.

loading process. In the A-B or F-B stage of **Figure 2(a)**, the increase in {00.2} diffraction intensity indicates the heightened activity of the twinning mechanism during this stage. Conversely, in the B-E stage, the decrease in {00.2} diffraction intensity suggests the gradual dominance of detwinning, leading to the aforementioned S-shaped curve. Interestingly, from **Figure 3(b)**, it can be observed that the presence of precipitates does not fundamentally alter the alternating dominant microscale deformation mechanisms in the alloy.

4. Discussions

Diffraction experimental data and simulation models have provided initial insights into the twinning behavior of AXM10304, a precipitation-strengthened magnesium alloy, during cyclic loading. However, in addition to the de/twinning mechanisms, the dislocation slip mechanism also influences the macroscopic mechanical response of this alloy. Diffraction experimental data, unfortunately, cannot distinguish between the respective degrees of involvement of de/twinning and dislocation slip in the deformation process. Leveraging the calibrated EVPSC-TDT model, we further elucidated the relative activities of various microscale plastic deformation modes in this alloy during the cyclic loading process. This helps to deepen our understanding of the impact of microscale mechanisms on macroscopic mechanical responses and analyze the interplay between these microscale mechanisms and the precipitates. We selected the simulated data from the initial compression and the first cycle as representatives. As shown in **Figure 4**, the EVPSC-TDT model provides the evolution history of the four plastic deformation modes (prismatic slip, basal slip, pyramidal slip, and de/twinning) in both ST and PA specimens with respect to cyclic loading strain. For the ST specimens, the plastic deformation mode first activated during the initial compression stage is basal slip [see A-B in **Figure 4(a)**]. As local stresses within the grain increase, the RSS on the twinning shear plane becomes sufficient to activate the twinning mechanism. Simultaneously, prismatic slip also initiates. Near point B within initial compression, the TVF reaches its maximum at 3.47%. During the BC stage of the first cycle, plastic deformation is almost negligible, with basal slip becoming the dominant plastic deformation mechanism, resulting in a slight pseudoelastic release during the compression unloading stage. Next, during the tensional C-D stage, the de/twinning mode predominates, and the corresponding TVF begins to decrease, indicating that detwinning becomes the primary plastic deformation mechanism in this stage, which is consistent with the results in **Figure 3(a)**. In the D-E stage, the TVF has reduced to nearly zero, indicating that the twins generated during the compression stage have been almost completely consumed by the detwinning mechanism. Detwinning ceases to be effective, and prismatic slip begins to dominate. Due to prismatic slip becoming the dominant hardening mode in the D-E stage of 1st cycle, and considering its relatively high CRSS, a higher external stress is required to accommodate plastic deformation, resulting in the secondary hardening effect

during the tension stage [see **Figure 2(a)**]. Similar to the B-C stage, the E-F stage is an unloading process characterized by minimal basal slip, leading to a less pronounced pseudo-elastic release [10]. The microscale mechanism evolution during the reverse compression stage of the first cycle (F-B) is similar to that of the initial compression stage. As the TVF begins to increase during this stage, it indicates that twinning becomes the dominant plastic deformation mode. It is noteworthy that, as some parent grains have completed the nucleation process, twinning growth predominates. The latter has a relatively lower CRSS, resulting in a higher TVF rate and an increase in the TVF at point B. Additionally, due to the longer duration of twinning growth (the compression process from F to B is longer than A to B), this leads to a higher TVF at the end of the first cycle compared to the end of the initial compression stage.

Figure 4(b) illustrates the evolutionary history of various plastic deformation mechanisms during the initial compression and the first cycle in PA sample with respect to cyclic strain. Once again, the simulation results confirm that the coherent precipitates do not fundamentally alter the evolution of various finite plastic deformation modes, as illustrated in section 3. Certainly, the presence of precipitates still exerts an influence on microscale behavior. Looking at the A-B stage, it is evident that the twinning mechanism is significantly more active in the PA sample. Comparing the initial CRSS, τ_0^{α}, the twinning nucleation CRSS,

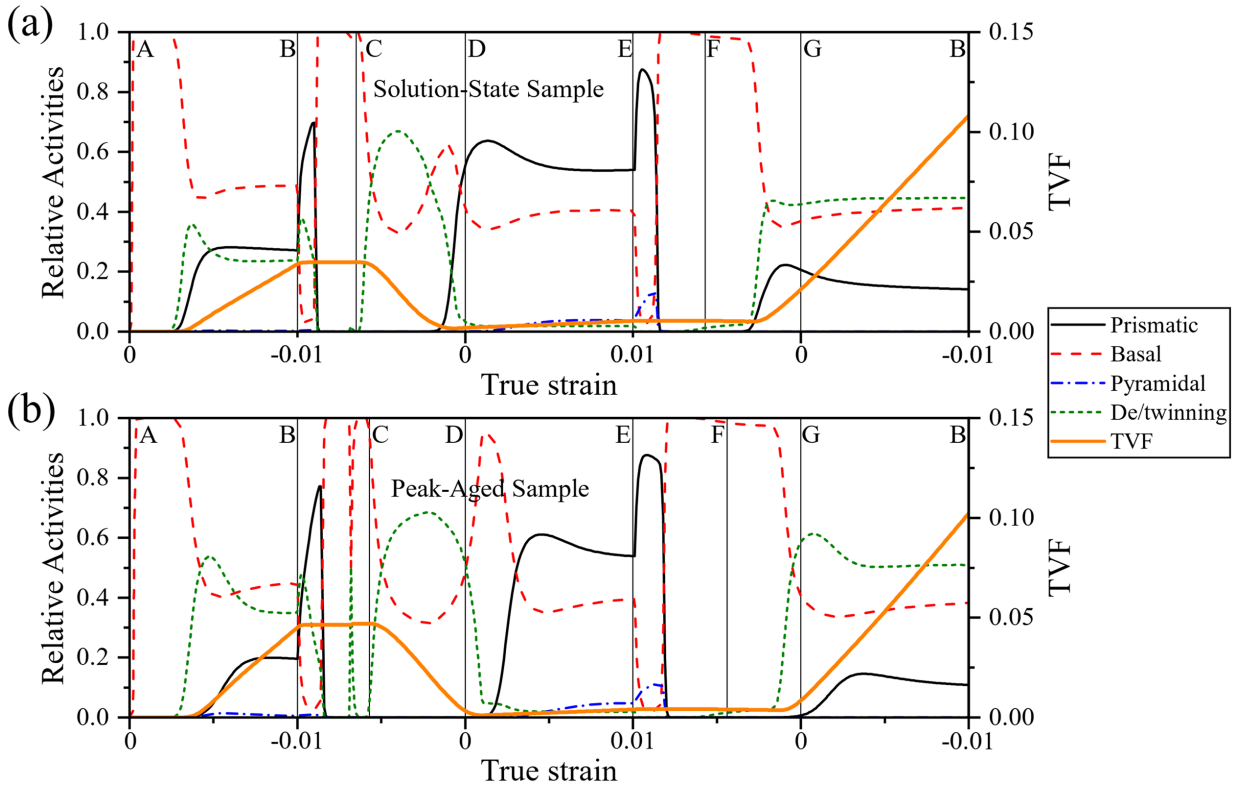

Figure 4. The predicted evolution of the relative activities of the prismatic slip, basal slip, pyramidal slip, and de/twinning during the initial compression and the first cycle with respect to cyclic loading strain for the (a) ST sample and (b) PA sample.

τ_0^{ini}, in PA specimens increases by 13.04% due to the strengthening effect of coherent precipitates, while the τ_0 for prismatic slip increases by a remarkable 34.72%. This makes the twinning nucleation mechanism more favorable in the initial compression stage for the PA specimens, resulting a larger maximum TVF (~4.65%) at point B of initial compression. However, at the end of the first cycle, the maximum TVF for the PA sample shows a slight decrease, measuring 10.22%, while the ST sample exhibits a maximum TVF of 10.82%. This result is attributed to the presence of precipitates causing an increase in the CRSS for twinning growth in the PA sample within G-B stage, resulting in a reduction in the TVF rate and a decrease in the maximum TVF at point B. In the other stages of the first cycle, PA sample did not exhibit relative activities of plastic modes significantly different from that of ST sample. However, due to the strengthening effect of precipitates, the CRSS of various plastic deformation modes has increased, resulting in an increase in work hardening and peak stress for the PA sample.

To further elucidate the influence of precipitates on the de/twinning mechanism, the EVPSC-TDT model also predicted the maximum and residual TVF for the first ten cycles, as shown in **Figure 5**. It can be observed that, except for the initial compression, both the maximum and residual TVF of the ST sample are significantly higher than those of the PA sample. Taking the 10th cycle as an example, the maximum and residual TVF for the ST sample are 34.06% and 26.51%, respectively, while, at the same point, the corresponding TVF for the PA

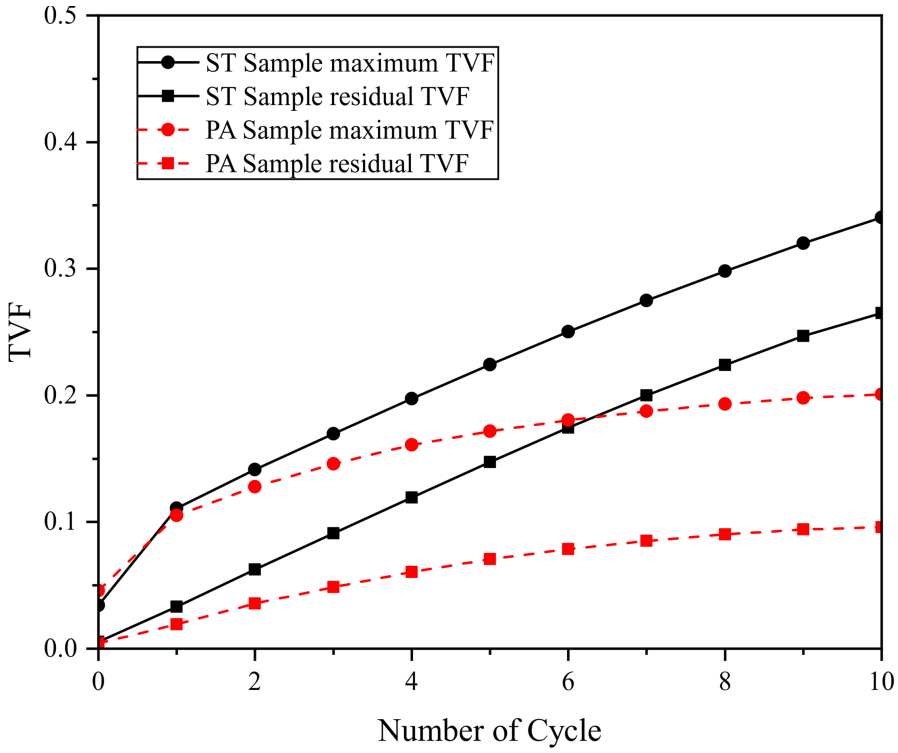

Figure 5. The predicted maximum and residual TVF as a function of number of cycle for the first 10 cycles.

sample are only 20.07% and 9.59%. From the perspective of the maximum TVF, the presence of precipitates increases the CRSS for twinning growth, reducing the ability of the twinning mechanism to accommodate plastic deformation, leading to a relatively smaller maximum TVF in the PA sample. Additionally, the detwinning mechanism in the PA specimens consumes more twins compared to the ST specimens, resulting in a lower residual twin. From **Table 1**, the initial CRSS increments for basal slip, prismatic slip, and detwinning in the PA sample are denoted as 50%, 34.72%, and 15.79%, respectively. Therefore, in the C-D stage, the detwinning mechanism in the PA specimen is more preferred compared to the ST specimen, resulting in a higher consumption of pre-existing twins and a much smaller residual TVF.

5. Conclusion

Through the EVPSC-TDT model, this work reveals the evolution of the microstructural deformation mechanisms of extruded precipitation-strengthened magnesium alloy AXM10304 during multi-cycle loading and establishes their connection with macroscopic mechanical responses. Experimental and simulation results indicate that the tensile-compressive asymmetry of this alloy arises from the alternating dominance of twinning and detwinning mechanisms during the compression and tension processes, respectively. The presence of precipitates does not fundamentally alter this mechanism. Furthermore, the model reveals the influence of precipitates on various plastic deformation modes. The modeling results indicate that the presence of coherent precipitates inhibits the twinning mechanism during the compression stage. However, in the reverse tension stage, the detwinning mechanism is slightly promoted. Additionally, the precipitates strengthen various plastic deformation modes, resulting in increased work hardening during both the compression and the tensile secondary hardening stages, leading to higher peak stresses. This work contributes to understanding the cyclic loading mechanical behavior of magnesium alloys and provides guidance for the mechanical performance modulation of precipitation-strengthened magnesium alloys.

Acknowledgements

HW was supported by the National Natural Science Foundation of China (No. 51975365).

Conflicts of Interest

The authors declare no conflicts of interest regarding the publication of this paper.

References

[1] Xu, T., Yang, Y., Peng, X., Song, J. and Pan, F. (2019) Overview of Advancement and Development Trend on Magnesium Alloy. *Journal of Magnesium and Alloys*, **7**, 536-544. https://doi.org/10.1016/j.jma.2019.08.001

[2] Peng, Q., Ma, N., Li, X. and Zhang, J. (2012) Age Hardening Response of a Mg-5wt.%Sc Alloy under an Applied Stress Field. *Materials Letters*, **78**, 58-61. https://doi.org/10.1016/j.matlet.2012.03.063

[3] Agnew, S.R., Mulay, R.P., Polesak, F.J., Calhoun, C.A., Bhattacharyya, J.J. and Clausen, B. (2013) *In Situ* Neutron Diffraction and Polycrystal Plasticity Modeling of a Mg-Y-Nd-Zr Alloy: Effects of Precipitation on Individual Deformation Mechanisms. *Acta Materialia*, **61**, 3769-3780. https://doi.org/10.1016/j.actamat.2013.03.010

[4] Rosalie, J.M., Somekawa, H., Singh, A. and Mukai, T. (2012) The Effect of Size and Distribution of Rod-Shaped Precipitates on the Strength and Ductility of a Mg-Zn Alloy. *Materials Science and Engineering*: *A*, **539**, 230-237. https://doi.org/10.1016/j.msea.2012.01.087

[5] Pahlevanpour, A.H., Behravesh, S.B., Adibnazari, S. and Jahed, H. (2019) Characterization of Anisotropic Behaviour of ZK60 Extrusion under Stress-Control Condition and Notes on Fatigue Modeling. *International Journal of Fatigue*, **127**, 101-109. https://doi.org/10.1016/j.ijfatigue.2019.05.030

[6] Wu, B.L., Duan, G.S., Du, X.H., Song, L.H., Zhang, Y.D., Philippe, M.J., *et al.* (2017) In Situ Investigation of Extension Twinning-Detwinning and Its Effect on the Mechanical Behavior of AZ31B Magnesium Alloy. *Materials & Design*, **132**, 57-65. https://doi.org/10.1016/j.matdes.2017.06.023

[7] Guillemer, C., Clavel, M. and Cailletaud, G. (2011) Cyclic Behavior of Extruded Magnesium: Experimental, Microstructural and Numerical Approach. *International Journal of Plasticity*, **27**, 2068-2084. https://doi.org/10.1016/j.ijplas.2011.06.002

[8] Dong, S., Yu, Q., Jiang, Y., Dong, J., Wang, F., Jin, L., *et al.* (2017) Characteristic Cyclic Plastic Deformation in ZK60 Magnesium Alloy. *International Journal of Plasticity*, **91**, 25-47. https://doi.org/10.1016/j.ijplas.2017.01.005

[9] Briffod, F., Shiraiwa, T. and Enoki, M. (2020) Monotonic and Cyclic Anisotropies of an Extruded Mg-Al-Ca-Mn Alloy Plate: Experiments and Crystal Plasticity Studies. *Materials Science and Engineering*: *A*, **772**, Article ID: 138753. https://doi.org/10.1016/j.msea.2019.138753

[10] Xie, D., Lyu, Z., Li, Y., Liaw, P.K., Chew, H.B., Ren, Y., *et al.* (2021) In Situ Monitoring of Dislocation, Twinning, and Detwinning Modes in an Extruded Magnesium Alloy under Cyclic Loading Conditions. *Materials Science and Engineering*: *A*, **806**, Article ID: 140860. https://doi.org/10.1016/j.msea.2021.140860

[11] Xie, D., Li, Z.H., Sasaki, T.T., Gao, Y.F., Lyu, Z.Y., Feng, R., *et al.* (2023) Identifying the Effect of Coherent Precipitates on the Deformation Mechanisms by in Situ Neutron Diffraction in an Extruded Magnesium Alloy under Low-Cycle Fatigue Conditions. *Acta Materialia*, **251**, Article ID: 118903. https://doi.org/10.1016/j.actamat.2023.118903

[12] Li, H., Kang, G. and Yu, C. (2020) Modeling Uniaxial Ratchetting of Magnesium Alloys by a New Crystal Plasticity Considering Dislocation Slipping, Twinning and Detwinning Mechanisms. *International Journal of Mechanical Sciences*, **179**, Article ID: 105660. https://doi.org/10.1016/j.ijmecsci.2020.105660

[13] Lee, S.Y., Wang, H., Gharghouri, M.A., Nayyeri, G., Woo, W., Shin, E., *et al.* (2014) Deformation Behavior of Solid-Solution-Strengthened Mg-9 Wt.% Al Alloy: *In Situ* Neutron Diffraction and Elastic-Viscoplastic Self-Consistent Modeling. *Acta Materialia*, **73**, 139-148. https://doi.org/10.1016/j.actamat.2014.03.038

[14] Nakata, T., Xu, C., Ajima, R., Shimizu, K., Hanaki, S., Sasaki, T.T., *et al.* (2017) Strong and Ductile Age-Hardening Mg-Al-Ca-Mn Alloy That Can Be Extruded as Fast as Aluminum Alloys. *Acta Materialia*, **130**, 261-270.

https://doi.org/10.1016/j.actamat.2017.03.046

[15] Wang, H., Wu, P.D., Tomé, C.N. and Huang, Y. (2010) A Finite Strain Elastic-Viscoplastic Self-Consistent Model for Polycrystalline Materials. *Journal of the Mechanics and Physics of Solids*, **58**, 594-612. https://doi.org/10.1016/j.jmps.2010.01.004

[16] Wang, H., Wu, P.D., Tomé, C.N. and Wang, J. (2012) Study of Lattice Strains in Magnesium Alloy AZ31 Based on a Large Strain Elastic-Viscoplastic Self-Consistent Polycrystal Model. *International Journal of Solids and Structures*, **49**, 2155-2167. https://doi.org/10.1016/j.ijsolstr.2012.04.026

[17] Wang, H., Clausen, B., Tomé, C.N. and Wu, P.D. (2013) Studying the Effect of Stress Relaxation and Creep on Lattice Strain Evolution of Stainless Steel under Tension. *Acta Materialia*, **61**, 1179-1188. https://doi.org/10.1016/j.actamat.2012.10.027

[18] Zhang, X., Zhou, K., Wang, H., Jiang, Y., Sun, X., Liu, C., *et al.* (2023) On the Cyclic Torsion Behavior of Extruded AZ61A Magnesium Alloy Tube. *International Journal of Fatigue*, **174**, Article ID: 107704. https://doi.org/10.1016/j.ijfatigue.2023.107704

[19] Qiao, H., Agnew, S.R. and Wu, P.D. (2015) Modeling Twinning and Detwinning Behavior of Mg Alloy ZK60A during Monotonic and Cyclic Loading. *International Journal of Plasticity*, **65**, 61-84. https://doi.org/10.1016/j.ijplas.2014.08.010